A Detection Method of Dot Patterns and Its Application to Fluorescent Dots Counting

Yongping Zhang, Dechun Zheng, Zhongkun He

School of Electronic and information Engineering, Ningbo University of Technology, Ningbo, 315016，China

***Abstract* — In this paper, a two-step refining method is proposed to perform dot pattern detection. Firstly, the linear structures are suppressed and the candidate dot patterns are found by using the morphological filters in combination with automatic thresholding technique. Secondly, the genuine dot patterns are detected by employing a kind of multiscale contrast measure. This refining method reduces the detection of light dot to the detection of a single point that is located approximately in the center of each dot. The counting procedure is then largely simplified. Some computational results have been presented to demonstrate the performance of the detection algorithm. Further development of the method allows its application to more general texture image analysis.**

Keywords - Dot patterns Detection; Multiscale contrast; TopHat filtering; Texture analysis

I. NTRODUCTION

Dots detection and counting techniques have been applied to a wide range of areas, such as virus detection, disease diagnosis, dynamics of intracellular networks, gene mapping, DNA replication and recombination, and cell-cell interaction [1-17]. To the typical fluorescent image of cells, a convenient counting method is manual through visual inspection under the microscope or from captured images. Most of the time, those dots are visible to the human eye and can be correctly counted by manual method. But some dots with small size or weak signal-to-noise ratio render their observation difficult even with high-resolution microscopy. Moreover, the manual counting process is time-consuming and laborious. Therefore, developing a tool to automate the process of dots counting is essential to overcome the disadvantages of visual analysis.

Generally, there are two important structures in a fluorescent image of cells: one is the light dots; the other one is the light boundaries between the cells (see Fig.1). Therefore, the main task of fluorescent image analysis is to detect the cells in the image and to count the number of dots per cell. Such detection problem of cells and dots is virtually a classical image segmentation problem.

Image segmentation is the process of partitioning an image into several segments. An important goal of segmentation is to simplify the representation of image information, being conductive to further processing such as object description or recognition. In practice, image segmentation can be also seen as the classification process of assigning each to one of the image compositions by a rule.

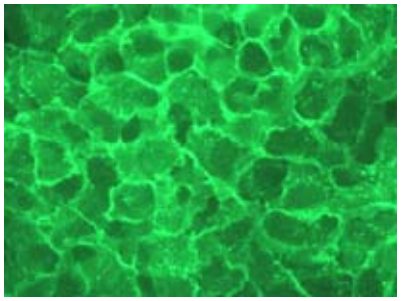

Fig.1 Scaled fluorescent image. A431 (vulval carcinoma) cells stimulated with epidermal growth factor (EGF) beads. The size of the image is 640×480

Existing image segmentation methods can be broadly divided into five types: edge detecting methods, shape-based methods, threshold-based or clustering methods, region growing methods, and hybrid methods [18]. These methods can also be categorized as: (1) edge-based and (2) region-based. Edge-based approaches partition an image by taking the edge information into account. In region-based approaches, an image is divided into different groups of pixels according to a certain similarity criterion. Many image segmentation approaches are intended for specific application fields to yield better results, for example, real-time image segmentation, color image segmentation, 3-D image segmentation, and motion image segmentation.

In previous works, some feature-based segmentation and recognition techniques have been adopted to realize the automation of dots counting. By extracting some distinguished features of dot patterns and implementing the procedure of classification, the dots counting was then automatically accomplished with the aid of computer. The

features derived from the input image, including geometric, texture and spectral, have been devoted to describing dot patterns. Statistical analysis (e.g. [15]), neural networks (e.g. [16]) and fuzzy clustering (e.g. [17]) have been employed to classify dot features. In the current study, we present a two-step refining automated method to perform fluorescent dots detection. The main distribution of this work is that a multiscale contrast descriptor is developed for dot pattern detection.

Because the human visual system is more sensitive to the difference in luminance than absolute luminance, image contrast that measures the variation in intensity in a small, most or all region of an image has been used as one of the important features to descript visual images. The contrast defined on small neighborhoods of pixels is called local contrast, which can be employed as a tool to classify pixels and describe textures. Several approaches to the quantitative measures of local contrast have been provided in the past years. The work in [19] uses the mean gray values in two rectangular windows centered on a given pixel to measure local contrast. Based on a local analysis of edges, a measure of local contrast is defined in [20] and is derived from the definition in [19]. The variation in size of neighborhoods gives rise to a multiscale concept of contrast. Local multiscale methods have been proposed for image contrast enhancement [21] and [22].

Multiscale filters, like Laplacian of Gaussian (LoG) [23], Gabor wavelet [24], and the difference of Gaussian (DoG) [25-28] have been provided as exact point-spread function of neurons in visual pathway to describe the mechanisms selective for certain spatial frequencies in the input [29] and [30], and widely used in texture feature extraction, image segmentation, image indexing and retrieval [31-36]. DoG filters, so-called Mexican Hats in some literatures, are suitable for detecting shape features such as edges, bars, corners and dots because of their agreement with Gaussian derivatives. Our approach to dot pattern detection is based on local multiscale contrast, the modified DoG filter responses.

In this work, a two-step refining scheme is provided to perform the detection of light dots based on multiscale analysis in combination with TopHat filtering [37]. Morphological TopHat filtering followed by automatic thresholding is used to find the candidate dots. The local maximality of responses of the multiscale contrast descriptor is then employed as a criterion to classify the detected candidate dots. The method reduces the detection of light dot to the detection of a single point that positioned approximately in the center of the dot. This approach provides a way for the simplification of the dot counting procedure.

The paper is organized as follows: Section 2 depicts the multiscale method of dot pattern detection, and Section 3 presents the experimental results and discussions. Section 4 concludes the paper.

II. DOT PATTERN DETECTION

In this section, a combined approach to dot detection is developed on the basis of morphological filtering and multiscale analysis. The morphological Tophat transform is used to suppress linear structures and find candidate dots. A multiscale contrast detector is developed to refine the dot detection. Once the possible dot location is detected, each candidate dot is further classified using the detector with maximality and lateral inhibition criteria. The dots failed to meet the criteria are treated as the false-positive dots and will be taken away from the list of the valid dots. The flow diagram of dot pattern detection algorithm is shown in Fig. 2.

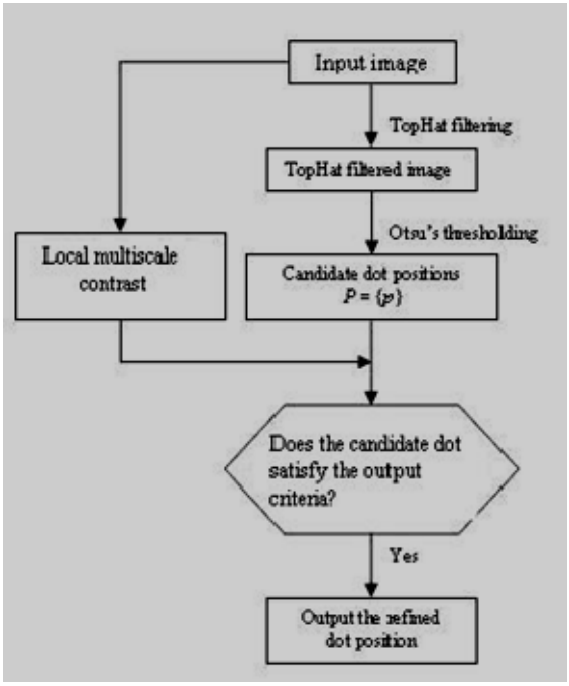

Fig.2 The flow diagram of dot pattern detection algorithm

A. Morphological Filtering

Linear structures such as the boundaries between cell zones must be removed for implementation of effective dot feature enhancement algorithm, although these structures are important for cell zone segmentation. Excluding all structures which are larger than a given linear distance in any direction is a way to achieve the goal. The grayscale area TopHat transform followed by constant or variable threshold is the most common technique for dot feature enhancement [37]. The transform is defined as the algebraic difference between an area opening and the original image I:

$$TopHat(I) = I - \max_{B}(\min_{B}(I)) \quad \textbf{Error! Reference source not found.}, \qquad (1)$$

where *B* is the neighborhood defined by a structure element. This filter allows the straightforward extraction of small light or dark structures regardless of their shapes.

To suppress the liner structures, a better solution is to use linear structuring element (i.e. a rectangle with a width of only one pixel). To exclude the most linear structures, generally, the eight TopHat filters corresponding to eight equally spaced angles are sequentially performed, and then thresholding is used. We find that regardless the threshold chosen many dots on the boundaries remain. Another drawback is that after thresholding, the number of pixels (or area) per dot is not uniform. Both will affect the accuracy of automated counting. In the next subsection, to overcome these disadvantages and ensure each candidate is fully delineated, a multiscale extracting algorithm is provided. Inspired by the shunting mechanism [26], a modified DoG (Difference of Gaussians) filter is introduced as multiscale contrast detector to detect dot patterns.

B. Contrast Descriptors

In this work, we use a modified DoG filter to detect the local contrast. The DoG filter can be defined as:

$$DoG_{\sigma,\lambda}(x,y) = G_{\sigma}(x,y) - G_{\lambda\sigma}(x,y) = \frac{1}{2\pi\sigma^2}\left(e^{-\frac{x^2+y^2}{2\sigma^2}} - \frac{1}{\lambda^2}e^{-\frac{x^2+y^2}{2\lambda^2\sigma^2}}\right)$$

Error! Reference source not found. (2)

where λ is a positive constant.

We define the local contrast of the input image *I* at position $p = (x, y)$ as:

$$C_{\sigma,\lambda}(I,p) = C_{\sigma,\lambda}(I,x,y) = \frac{U_{\sigma,\lambda}(I,x,y)}{1+I_{\sigma}(x,y)+I_{\lambda\sigma}(x,y)} = \frac{\max(0, DoG_{\sigma,\lambda} * I(x,y))}{1+G_{\sigma} * I(x,y)+G_{\lambda\sigma} * I(x,y)} \quad (3)$$

If the parameter λ is fixed, we simply denote by DoG_{σ} and C_{σ} the filter $DoG_{\sigma,\lambda}$ and the contrast $C_{\sigma,\lambda}$.

As an example, we perform local contrast detection on the image shown in Fig. 1. In the experiments, fixed value of λ =2 is used. The responses of detectors with σ = 0.52 and σ = 1.04 are shown in Fig. 3(a) and (b), respectively. As can be seen from the computational example, the response of contrast detector to the original image not only enhances the dot patterns, but it also enhances the boundaries. Hence the direct use of contrast detector to an input image cannot effectively accomplish the detection task. In subsection 2.3 we will propose a combined method to solve the problem.

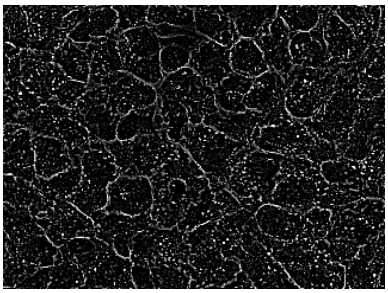

(a)

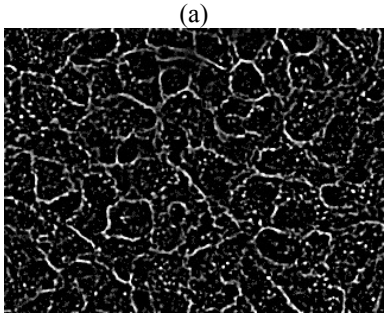

(b)

Fig.3 Local contrast of image Fig. 1: (a) the response of detector with σ = 0.52; (b) the response of detector with σ = 1.04

C. Dot Pattern Detection Algorithm

In this subsection, we propose an algorithm for the effective detection of dot patterns. The algorithm consists of the following steps:

Step 1: Sequentially apply TopHat filters with linear structuring elements, which correspond to eight directions (0, π/8, π/4, 3π/8, π/2, 5π/8, 3π/4 and 7π/8), to the input image $I(x, y)$. Let the filtered image be $TH(x, y)$.

Step 2: Threshold the filtered image $TH(x, y)$. The global threshold is determined using Otsu's algorithm [30]. Let the resultant binary image be $f(x, y)$, which gives the possible dot domain:

$$P = \{(x, y) \mid f(x, y) = 1\}.$$

Step 3: Apply the multiscale detector C_{σ} to $I(x, y)$ on the domain *P* to detect the maximality and the lateral inhibitory. For each candidate pixel *p*, the local maximality of the contrast is defined as:

$$C_{\sigma}^{M}(p) = \begin{cases} 1, & if \quad C_{\sigma}(p) >= C_{\sigma}(q) \quad for \quad all \quad q \in N_{3\times3}(p) \\ 0, & otherwise \end{cases} \quad (4)$$

where $N_{3\times3}(p)$ is the 3×3-neighborhood of pixel *p*. Similarly, the lateral inhibitory in distance *d* (it should be equal to or larger than the radius *r* of the positive support set of the function DoG_{σ}, and equal to or less than the half of the average distance between dots) is defined as:

$$C_\sigma^I(p) = \begin{cases} 1, & if \quad \frac{1}{2}C_\sigma(p) > C_\sigma(q), \quad \forall q : dist(p,q) = d \\ 0, & otherwise \end{cases} \quad (5)$$

where d is Proportional to the maximum of distances between the centers of dots.

Step 4: Classify the candidate dots according to the multiplication of $C_\sigma^M(p)$ and $C_\sigma^I(p)$. If $C_\sigma^M(p) \cdot C_\sigma^I(p) = 1$, output the real dot position p.

By combining the detection results corresponding to different standard deviations together, a multiscale detection strategy is obtained. The above algorithm reduces the detection of a light dot to the detection of a single point that is located approximately in the center of the dot. This approach can greatly simplify the procedure of dot counting.

D. Selection of Parameters

In order to faithfully detect dot patterns, the standard deviation σ must be carefully selected. For a faithful contrast detector, its positive support set (center region) should cover the light dot. Assuming that the radius of light dots is r, the radius of the positive support set of the function DoG_σ should be selected as r. That is, the distance from the zero crossing where the function DoG_σ changes polarity to the original point should be r. From $DoG_\sigma = 0$, we have

$$e^{-\frac{r^2}{2\sigma^2}} - \frac{1}{\lambda^2} e^{-\frac{r^2}{2\lambda^2\sigma^2}} = 0. \quad (6)$$

Solving the above equation,

$$\sigma = \frac{r}{2\lambda}\sqrt{\frac{\lambda^2 - 1}{\ln \lambda}}. \quad (7)$$

When the value of parameter λ is fixed as 2, we have

$$\sigma \approx 0.52r. \quad (8)$$

Hence the parameter σ can be determined by the distribution of dots' sizes according to formula (8). To detect dots with diameter 3, for example, the standard deviation σ may be chosen as 0.52.

The parameter d depends on the minimum distance between dot centers. In this approach, it is settled as the average of dots' radii.

Fig. 4 shows an example of dot pattern detection using the combined algorithm. In the experiments, four different values of standard deviation σ (= 1.56, 2.08, 2.60, 3.12), which correspond to four different values of radius r = 3, 4, 5 and 6, are selected to perform dot detection. The size of the original image is 2560×1920 pixels. The detected dot centers are marked with black points. 3267 dots are detected. The part of the image in Fig. 4 (a) denoted by the white rectangle is displayed at higher magnification in Fig. 3 (b). Subsequently, the boxed area in Fig. 4 (b) is shown at higher magnification in Fig. 4 (c).

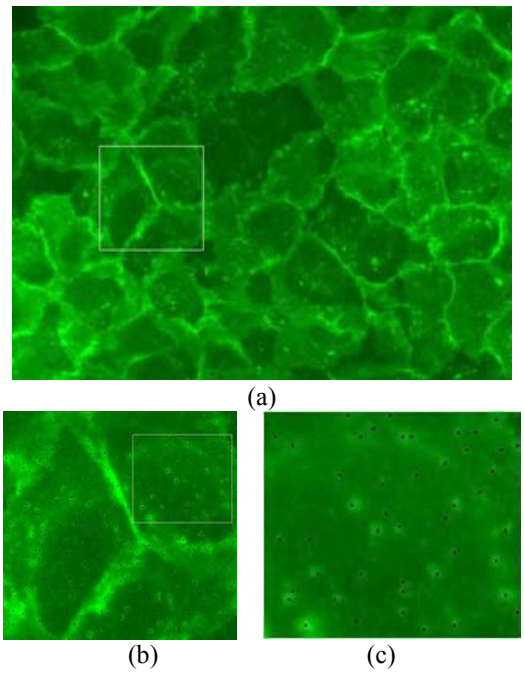

(a)

(b) (c)

Fig.4 Detection experiments. (a) Fluorescent image of A431 cells stimulated with EGF beads. Its size is 2560×1920 pixels. Detected dot centers are marked with black points. 3267 dots are detected. (b) Higher magnification of the part of the image in (a) denoted by the white rectangle. (c) The boxed area in (b) is shown at higher magnification

III. RESULTS AND DISCUSSIONS

The present approach is motivated by the development of automatic detection solution for dot patterns in various fluorescent images. The goal of the dot detection algorithm is to generate counts of dots within specimen of interest that are close to that obtained by manual counting. The manual count value, which is known as ground truth, is compared with the results of the automatic detectors.

A. Evaluation of Performance

For validation of the algorithm, each image was manually counted three times independently, and the average of these results is used as the final manual counting result. Since most images of A431 cells stimulated with EGF may include more than a thousand dots, like the image shown in Fig. 1 which includes about 2500 dots (2568 dots are detected using our automated counting method), visual observation and manual counting are very time-consuming. To guarantee the effective implementation of manual counting, only 20 smaller images (1024×1024) of A431 with EGF beads are used to obtain the ground truth in this approach. By applying the automated method, some false positions (false-positive dots) have been detected. The

number of these positions is about 4.62 percent of the total number counted by automatic method. The false positions are detected by automated analysis but rejected in manual counting because of their being the corner points on the bright boundaries between cells. Meanwhile, some real positions (true-negative dots) are still missed because of their extremely large areas or lower intensities. The number of the true-negative dots is about 2.91 percent of the total number counted by manual method. This means that more that 97 percent of real dots have been correctly detected. The summary of test result is shown in Fig. 5. The correlation coefficient between the manual and automated methods is 0.98529. This indicates that the current dot detection method gives valid results.

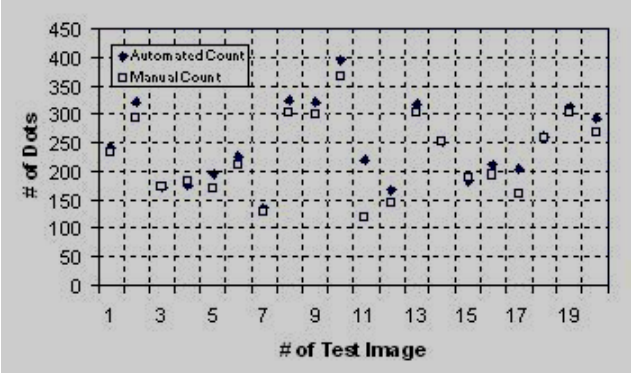

Fig.5 Comparison of manual and automated dot counts for twenty images of 1024×1024

B. *Comparison with Intensity-based Method*

The performance of the present dot detection method is further analyzed by carrying out a classification results comparison. In [15] the total intensity was used to classify the candidate dots gotten by the TopHat filtering. Let $I_{\max}$ be the maximum intensity within the dot mask (here is a 5×5 window), γ be a constant (here 0.33). The total intensity is defined as the sum of the intensities that are larger than $\gamma I_{\max}$ and is given by

$$I_{tot} = \sum_{(x,y)\in dotmask} I(x,y)clip(I(x,y) - \gamma I_{\max}) \quad (9)$$

where

$$clip(u) = \begin{cases} 1 & u \geq 0 \\ 0 & else. \end{cases} \quad (10)$$

For classification of candidate dots, a training set of the detected dots is selected to determine an interval of values of the feature I_{tot}. The interval is defined from the minimum value to the maximum value of that feature as observed in the training set which consists of real dots. Fig. 6 shows the results detected by the present method and the total intensity-based method. As can be seen from this figure, almost all the dots perceptible by visual inspection were correctly identified by both methods. Using the contrast detector, the output is approximately in the center of dot and most hidden dots have been detected. Using the total intensity-based method, the most pixels of a dot have been detected; the sizes of dots detected by the method distribute over a wider range; to accomplish the dot counting task, a labeling procedure must be adopted to the classified results.

On the other hand, using the total intensity-based method, the detection performance depends upon the selection of a training set. It is then not suit for fully-automated dot pattern detection.

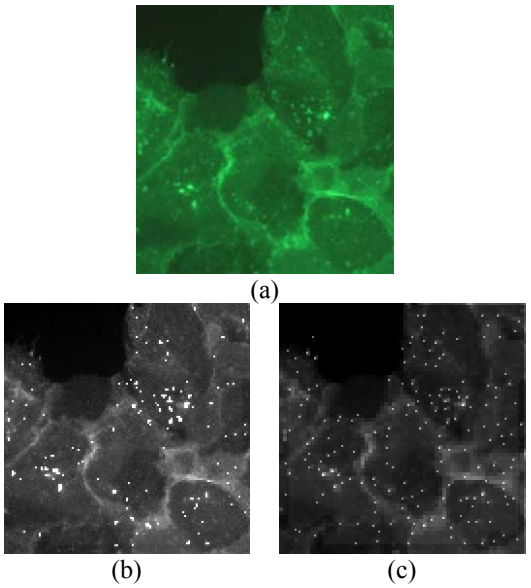

Fig.6 Comparison of dot detection methods: (a) the original image of A431 with EGF beads; (b) the dot detecting results using total intensity-based method; (c) the dot detecting results using present multiscale method

C. *Application to Cell Detection*

We applied the combined method to detection of cat retina cells. Fig. 7 (a) shows a confocal image of cat retina, which is downloaded from [38] (thanks). The cells in the image form two groups: the group A is called outer nuclear layer (ONL) and the group B is called inner nuclear layer (INL). Here only the cells in the ONL are counted. Using the combined dot detection algorithm, 604 cells are detected. The detected cell centers are marked with red color. Compared with manual counts (618 cells), the absolute error is 2.2%.

IV. CONCLUSİON

We have developed a fully-automated algorithm for dot pattern detection from fluorescent scanning images based on a contrast filter bank, which is a multiscale family of modified DoG filters. For reducing the false positions, the TopHat filters were used to find the candidate dots in

advance. The local maximality and lateral inhibition mechanism were introduced as the criteria to control the outputs of the contrast filters.

We compared the conventional total intensity-based analysis and the presented method. The result indicated that our method is more direct and effective. Also, we compared the visual observation and the automated analysis of dot patterns. A good correlation between the dot counts was observed. By applying the dot detection algorithm, more than 97 percent of light dots have been correctly detected in spite of the irregularities in dot shape, since isotropic contrast operator was adopted as the dot detector. The presented method has the advantages of simplicity and reliability in detecting dot patterns.

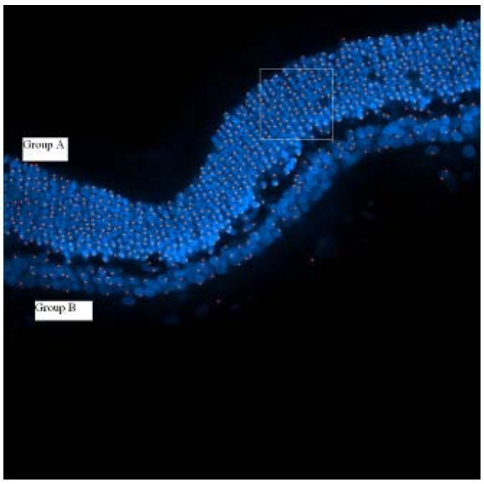

(a)

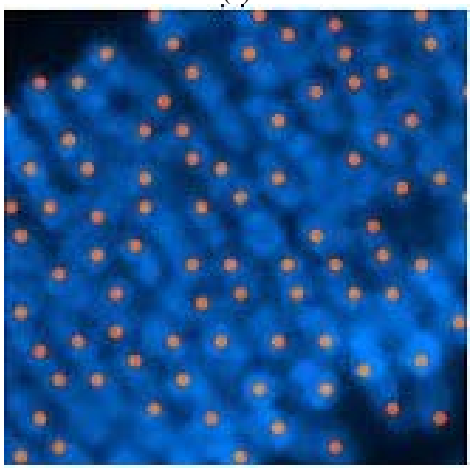

(b)

Fig.7 Cell detection. (a) Cat retina image 3d.cat.topro.z1-0001.tif from [43]. Detect cell centers are marked with red color. The boxed area in (a) is shown in (b) at higher magnification. 604 cells are detected in group A with 2.2% error compared with manual counts (618 cells)

ACKNOWLEDGEMENT

This research is partially supported by NSFC of Zhejang Province (No. LY13F020014).

REFERENCES

[1] X. Michalet, F. F. Pinaud, L. A. Bentolila, J. M. Tsay, S. Doose, J. J. Li, G. Sumdaresan, A. M. Wu, "Quantum Dots for Live Cells, in Vivo Imaging, and Diagnostics," Science, Vol. 307, pp. 538-544, 2005

[2] M. Massey, M. Wu, E. Conroy, W. Algar, "Mind Your P's and Q's: the coming of age of semiconducting polymer dots and semiconductor quantum dots in biological applications," Current opinion in Biotechnology, Vol. 34, pp. 30-40, 2015

[3] E. Petryayeva, I. Mdintz, W. Algar, "Quantum dots in bioanalysis: a review of applications across various platforms for fluorescence spectroscopy and imaging," Application Spectroscopy, Vol. 67, pp. 215-252, 2013

[4] T. Vu, W. Lam, E. Hatch, D. Lidke, "Quantum dots for quantitative imaging: from single molecules to tissue," Cell and Tissue Research, Vol. 360 (1), pp. 71-86, 2015

[5] D. Sage, F. R. Neumann, F. Hediger, S. M. Gasser, M. Unser, "Automatic tracking of individual fluorescence particles: application to the study of chromosome dynamics," IEEE Trans. on Image Processing, Vol. 14(9), pp. 1372-1383, 2005

[6] T. Ylikomi, O. Yli-Harja, T. O. Jalonen, "Quantification of vesicles in differentiating human SH-SY5Y neuroblastoma cells by automated image analysis," Neuroscience Letters, 396, pp. 102-107, 2006

[7] S. Yamaoto, Y. Nakajima, S. Tamura, Y. Sata, S. Harino, "Extraction of fluorescent dot traces from a scanning laser ophthalmoscope image sequence by spatio-temporal image analysis: Gabor filter and radon transform filtering, " IEEE Trans. on Biomedical Engineering, Vol. 46 (11), pp. 1357-1363, 1999

[8] P. Kahai, K. R. Namuduri, H. Thompson, "A decision support framework for automated screening of diabetic retinopathy," Int. Journal of Biomedical Imaging, Vol. 2006, pp. 1-8, 2006

[9] K. A. Goatman, M. J. Gree, J. A. Olson, J. V. Forrester, P. F. Sharp, "Automated measurement of microaneurysm turnover," Investigative Ophthalmology and Visual Science, Vol. 44 (12), pp. 5335-5341, 2003

[10] A. J. Frame, P. E. Undrill, M. J. Gree, "A comparison of computer based classification methods applied to the detection of microaneurysms in ophthalmic fluorescein angiograms," Computers in Biology and Medicine, Vol. 28 (3), pp. 225-238, 1998

[11] T. Spencer, J. A. Olson, K. C. McHardy, P. F. Sharp, J. V. Forrester, "An image –processing strategy for the segmentation of microaneurysms in fluorescent angiograms of the ocular fundus," Computers and Biomedical Research, 29, pp. 284-302, 1996

[12] F. Raimondo, M. A. Gavrielides, G. Karayannopoulou, K. Lyroudia, I. Pitas, I. Kostopoulos, "Automated Evaluation of Her-2/neu Status in Breast Tissue From Fluorescent In Situ Hybridization Images, " IEEE Trans. on Image Processing, Vol. 14 (9), pp. 1288-1299, 2005

[13] J. S. Ross, J. A. Fletcher, "The Her2/neu oncogene in breast cacer: prognostic factor, predictive factor, and target for therapy," Oncologist, 3, pp. 237-252, 1998

[14] J. Klijanienko, J. Couturier, M. Galut, A. K. El-Naggar, Z. Maciorowski, E. Padoy, V.Mosseri, P. Vielh, "Detection and quantization by fluorescence in situ hybridization (FISH) and image analysis of HER-2/neu gene amplification in breast cancer fine-needle samples," Cancer Cytopathol, Vol. 87 (5), pp. 312-318, 1999

[15] H. Netten, L. J. van Vliet, H. Vrolijk, W. C. R. Sloos, H. J. Tanke and I. T. Young, "Fluorescent dot counting in interphase cell nuclei," Bioimaging, 4, pp. 93-106, 1996

[16] B. Lerner, W. F. Clocksin, S. Dhanjal, M. A. Hulten, and C. M. Bishop, "Feature representation and single classification in fluorescence in-situ hybridization image analysis," IEEE Trans.

SMC---A: System and Human, Vol. 31(6), pp. 655-665, 2001.
[17] J. Selinummi, J.-R. Sarkanen, A. Niemisto, M.-L. Linne, T. Ylikomi, O. Yli-Harja and T. O. Jalonen, "Quantification of vesicles in differentiating human SH-SY5Y neuroblastoma cells by automated image analysis," Neuroscience Letters, 396, pp. 102-107, 2006.
[18] N. R. Pal and S. K. Pal, "A review on image segmentation techniques," Pattern Recognition, Vol. 26, no. 9, pp. 1277-1294, 1993.
[19] A. P. Dhawan, G. Buelloni, and R. Gordon, "Enhancement of mammographic features by optimal adaptive neighborhood image processing," IEEE trans. on Medical Imaging, Vol. 5(1), pp. 8-15, 1986.
[20] A. Beghdadi and A. Le Negrate, "Contrast enhancement technique based on local detection of edges," Computer Vision, Graphics, Image Processing, Vol. 46, pp. 162-174, 1989.
[21] T. Zong, H. Lin, and T. Kao, "Adpative local contrast enhancement method for medical images displayed on a video monitor," Med. Eng. Phys., vol. 22, pp. 79–87, 2000.
[22] E. Peli, "Contrast in complex images," J. Opt. Soc. Amer. A, vol. 7, pp. 2032–2040, 1990.
[23] D. Marr, "Early processing of visual information," Proc. Roy. Sot. London. B 275, pp. 483-534, 1976.
[24] J. Daugman, "Uncertainty relation for resolution in space, spatial frequency, and orientation optimized by two-dimensional cortical filters," J. 0pt. Soc. Amer. 2, pp. 1160-1169, 1985.
[25] H. Wilson and D. Gelb, "Modified line-element theory for spatial-frequency and width discrimination," J. Opt. Sot. Amer. Al, pp.124- 131, 1984.
[26] H. Neumann, Mechanisms of neural architecture for visual contrast and brightness perception. Neural Networks, 9(6), pp. 921-936, 1996.
[27] P. Kruizinga and N. Petkov, "Computational model of dot-pattern selective cells," Biological Cybernetics, **83** (4), pp. 313-325, 2000.
[28] D. Marr and E. Hildreth, "Theory of edge detection," Proceedings of the Royal Society of London, B(207): pp. 187-217, 1980.
[29] M. Sachs, J. Nachmias, and J. Robson, "Spatial frequency channels in human vision," J. Opt. Sot. Amer. 61, pp.1176- 1186, 1971.
[30] F. Campbell and J. Robson, "Application of Fourier analysis to the visibility of gratings," J. Physiology. 197, pp. 551-566, 1968.
[31] J. P. Antonie, D. Barache, R. M. Cesar and L. da Fontoura Costa, "Shape characterization with the wavelet transform," Signal Processing, 62, pp. 265-290, 1997.
[32] J. Malik, P. Perona, "Preattentive texture discrimination with early vision mechanisms," J Opt. Soc. Amer. A: Optics and Image Science 7(5), pp. 923-932, 1999.
[33] Y. Zhang, D. W. Fountain, R. M. Hodgson, J. R. Felenley and S. Gunetilike, "Towards automation of palynology 3: pollen pattern recognition using Gabor transforms and digital moments," J. Quaternary Science, 19(8), pp. 763-768, 2004.
[34] C. S. Tong, Y. Zhang and N. Zheng, "Variational image binarization and its multiscale realizations," J. Mathematical Imaging and Vision, 23, pp.185-198, 2005.
[35] Q. M. Tieng, W. W. Boles, "Recognition of 2D object contours using the wavelet transform zero-crossing representation," IEEE Trans. PAMI, 19(8), pp. 910-916, 1997
[36] J. Fayolle, L. Riou and C. Ducottet, "Robustness of a multiscale scheme of feature points detection," Pattern Recognition, 33(9), pp. 1437-1453, 2000.
[37] R. C. Gonzalez, R. E. Woods, Digital Image Processing, 2nd Edition, Upper Saddle River, NY: Prentice Hall, 2002.
[38] http://www.bioimage.ucsb.edu/byun-auto-cell-detect.php.